

Chapter 10

Neutron Imaging for Material Science and Engineering



P. S. Sarkar and Shefali Shukla

10.1 Introduction

Material science and engineering is an interdisciplinary area concerning the properties of matter and its application to various areas of science and engineering. The basic of all material science involves relating the material's desired properties and relative performances on a specific application to the structure of the atoms and phases in that material through characterization. Neutrons are sought for probing materials because they can provide bulk information, which is difficult to obtain using other techniques. Neutrons are very sensitive to light elements and can be used for their mapping even if they are encapsulated in high Z materials. The attenuation coefficients of various materials for neutrons also depend on the neutron energy, and this property has been exploited for Bragg neutron imaging for providing better contrast.

10.2 Major Applications of Neutron Imaging in Material Science and Engineering

This section deals with the applications of neutron imaging in various fields of material science ranging from flow field and degradation studies of proton exchange membrane (PEM) fuel cells to structural stability of hydrogen storage materials specifically essential for these type of fuel cells. Also like hydrogen, neutrons are very sensitive to lithium, enabling us to visualize lithium in lithium-ion batteries. Various aspects of Li-ion batteries preparation and operation have been covered.

P. S. Sarkar (✉) · S. Shukla
Technical Physics Division, Bhabha Atomic Research Centre, Mumbai 400085, India
e-mail: pss@barc.gov.in

S. Shukla
e-mail: shefali@barc.gov.in

An advanced kind of neutron imaging, namely Bragg-edge (already discussed in detail in the previous chapter) can also be used for crystalline imaging phases in materials. Residual stress measurement is of fundamental interest in order to estimate the service life of engineering components and structures subjected to various loading conditions operating in different environments. Neutron imaging application in residual stress measurements has an upper edge over the mechanical relaxation approaches such as the contour method or non-destructive methods such as X-ray diffraction.

10.2.1 Neutron Imaging of PEM Fuel Cells

Proton exchange membrane (PEM) fuel cells, which directly convert chemical energy to electrical energy, have attracted significant attention due to the numerous benefits they offer like high-power density, high energy conversion efficiency, fast start-up, low sensitivity to orientation and environmental friendliness. Figure 10.1 shows a schematic of a PEM fuel cell [1]. The heart of a PEM fuel cell is the membrane electrode assembly (MEA) which includes the membrane, the catalyst layers and the gas diffusion layers (GDL). Apart from MEA few more hardware components are incorporated in a fuel cell. They include gaskets for providing seal around the MEA to avoid leakage of gases and bipolar plates for assembling individual PEM fuel cells into a fuel cell stack and provide channels for the gaseous fuel and air. The membrane present between anode and cathode compartments serves as the electrolyte and helps conduct protons from the anode to the cathode.

One of the keys to PEM fuel cells (PEMFCs) performance and durability is water management. Water management in PEMFC is widely recognized to be a very complex issue, due to the fact that the gaseous reactants share the same pathways as the partly liquid product water. If the water evaporation is very slow, it will flood the membrane and the accumulation of water inside the field flow plate will impede the flow of oxygen into the cell, but if the water evaporates too fast, the membrane will be dry and the resistance across it increases. Both these cases are to be avoided to prevent degraded performance. For addressing the issue of water management, water distribution in the PEMFC must be accurately and efficiently measured for providing data for model validation. A typical PEMFC will be made up of 2 cm thick aluminium plate and about 1 cm thick graphite flow fields. The region of interest where water is present is very small around 5 mm which makes it difficult to measure water using conventional techniques like X-ray and magnetic resonance imaging. Neutron, however, can make the task easier as all the typical hardware of the fuel cell will be transparent to neutrons and only the hydrogenous part will be visible. Just by analyzing the neutron radiography images, the laminar water flow in an operating PEMFC can be measured.

Neutron imaging, therefore, has been used to investigate different aspects of water management, such as the effect of different flow field geometries, materials, operating

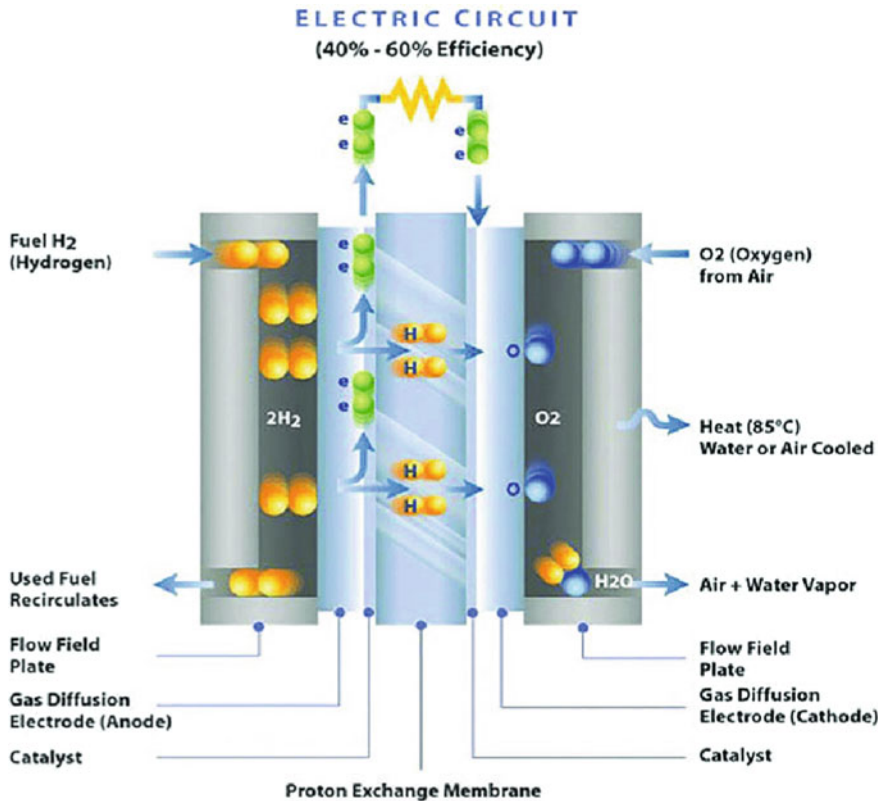


Fig. 10.1 Schematic of a PEM fuel cell [1] (open access)

conditions and degradation. In situ water content visualization for a commercial PEMFC has also been attempted using neutron imaging.

Totzke [2] conducted neutron radiography studies to examine flow field in prepared PEMFCs using a detector with a large FOV and high spatial resolution. The advantage of large FOV was that a complete fuel cell could be imaged in a single shot. Figure 10.2 shows the radiographs depicting the water evolution in the GDL and the flow field channels presented images have been normalized with respect to the reference image (dry cell). As the current density increases, the amount of water formed increases which is quite evident from (A), (B), (C) and (D).

Radiography images taken in trough plane direction were unable to separate the water distributions for the cathode and anode sides. Moreover, for actual analysis, data for fuel cell stacks were required. Since the water distribution may strongly differ between single cell and cell stacks, radiography studies had to be replaced by tomography studies to provide information on the water accumulations in individual cells of the stack. Markotter et al. [3] carried out quasi in situ tomography to study the water content in individual flow field channels of threefold stacks (Fig. 10.3).

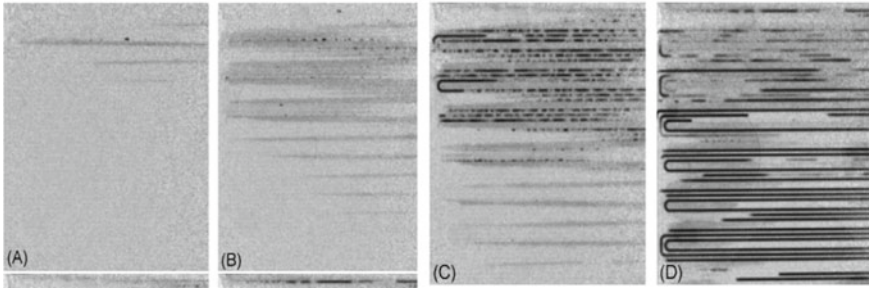


Fig. 10.2 Evolution of water distribution at different current densities, **a** after 30 min, $I = 100 \text{ mAcm}^{-2}$; **b** after 40 min, $I = 300 \text{ mAcm}^{-2}$; **c** after 65 min, $I = 400 \text{ mAcm}^{-2}$; **d** after 105 min, $I = 500 \text{ mAcm}^{-2}$ [2]. Reproduced with permission from Elsevier Copyright Clearance Centre

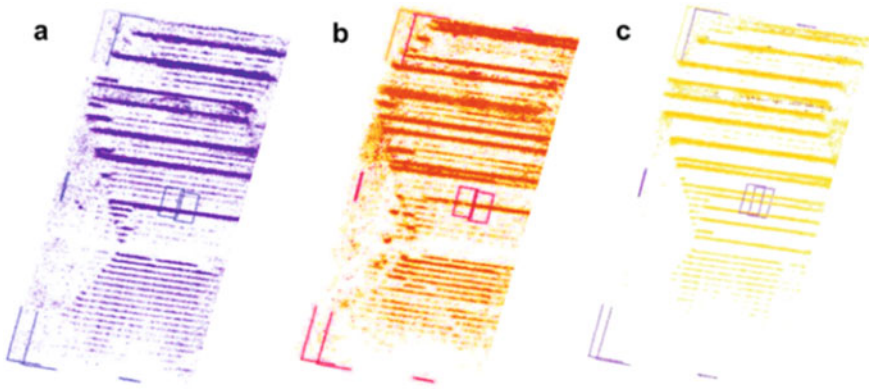


Fig. 10.3 Separated water distribution for each single cell in a threefold stack [3]. Reproduced with permission from Elsevier Copyright Clearance Centre

Fuel cells used for commercial applications have a flow field defined by discrete channel-land structures guiding the reactant gases. Sealing gaskets surround the flow field on its outer perimeter, separated from the flow field by an edge region. Gas and water transport between flow field and edge region strongly depend on the specific design of the fuel cell. Stahl [4] tried imaging water in this area because it could be subject to degradation effects.

Inside a gas diffusion layer (GDL), liquid water circulates under the effect of capillary forces from the catalyst layer (CL) to the flow channel. In the reverse direction, an optimum diffusivity of the reactant gases is required to sustain the electrochemical reaction with minimum mass transport losses. The simultaneous two-phase flow is maintained by the properties of the GDL, such as hydrophobicity, porosity or tortuosity [5]. Truhan et al. [6] studied through-plane water distribution and liquid removal in an actual operating fuel cell for different flow channel surface properties, using high-resolution neutron radiography. Biesdorf et al. [7] also evaluated the

impact of varying amounts of PTFE coatings inside the GDLs of polymer electrolyte fuel cells in relation to mass transport losses. Neutron radiography, limiting current density and pulsed gas analysis were used to obtain a detailed characterization of the local mechanisms and water distribution in GDL and CL. Figure 10.4 depicts the in-plane water distribution averaged during the first and last 30 min for the four configurations during continuous operation at full humidification.

Neutron imaging also allows studying the various mechanisms of fuel cell degradation, namely corrosion and ageing of GDL. The corrosion of carbonaceous components in PEMFCs is a concern for long-term durability. This corrosion can be as a result of potential excursions occurring during cycles of operation. Further, the transient power demands and localized water blockages can cause fuel starvation leading to favourable corrosive conditions. Carbon corrosion reduces efficiency of PEMFC through several mechanisms, and efforts are underway to find ways to reduce this phenomenon. Fairweather et al. [8] carried out studies to investigate the effect of cathode corrosion on through-plane water transport.

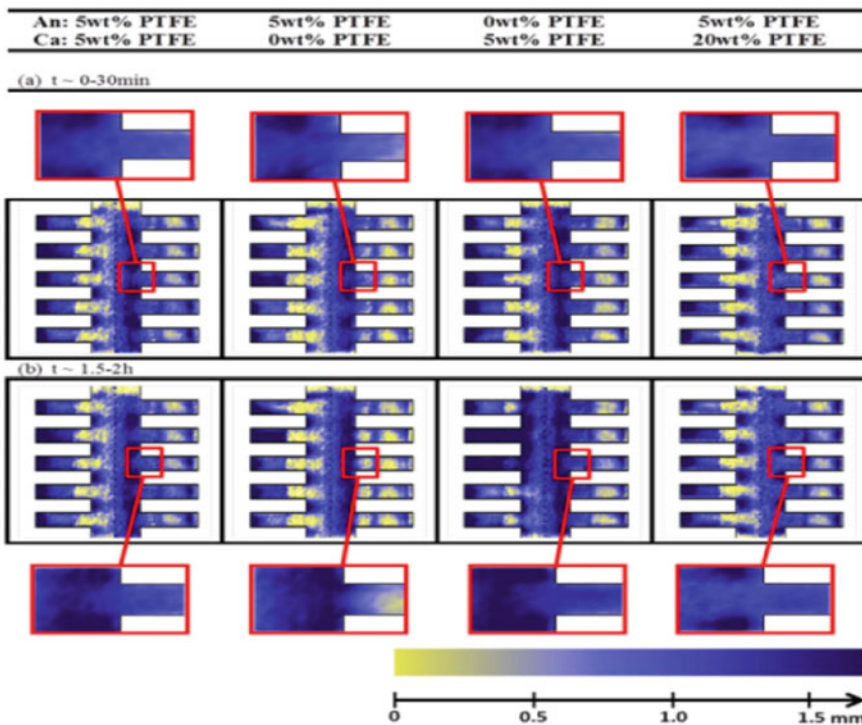
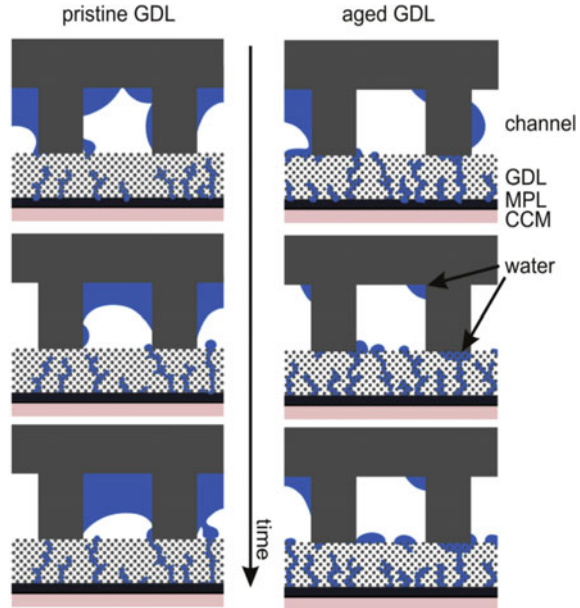


Fig. 10.4 In-plane water distribution averaged during the **a** first and **b** last 30 min for different coatings on anode and cathode during continuous operation at full humidification. The dotted line in the middle depicts the membrane, with its anode on the left and cathode on its right. The five fringes depict the gas channels of the flow field. The amount of water is represented in false colour code (yellow = dry, blue = wet) which corresponds to 0 and 1.7 mm water [7] (open access)

Fig. 10.5 Schematic illustration of possible water formation in a cell containing a new (left) or aged (right) GDL [9]. Reproduced with permission from Elsevier Copyright Clearance Centre



The membrane of the PEMFC must be sufficiently humidified to be proton conductive, but at the same time, too much water can clog the pores of GDL and obstruct the supply of reactant gases into the catalyst layer. During long-term operation due to GDL ageing, the water transport gets modified and this effect has been studied by several researchers. Katzel [9] used neutron imaging to study the effect of ageing of GDL on the water balance of the fuel cell. Figure 10.5 shows the schematic illustration of possible water formation in a cell containing a new or aged GDL. These inferences have been obtained from the neutron radiography results. As evident is that when the GDL ages, the hydrophobicity decreases and the water droplets accumulate on the GDL surface instead of on the channel walls. This water agglomerations on the aged GDL surface lead to modified water transport in the flow field and block the supply gases' path towards the catalyst layer. This results in less efficient water and gas transport which in turn affects the cell voltage.

10.2.2 Neutron Imaging for Hydrogen Storage Materials

Fossil fuel depletion and increase in energy consumption threaten the energy and economic security worldwide. In addition, fossil fuels are not environmentally friendly, so alternatives to fossil fuels are continuously being thought of. Hydrogen energy has long been proposed as hydrogen is the most abundant element on earth, and the by-products of energy production will be just water vapour (hydrogen cycle). Hydrogen also offers the advantage of a high chemical energy per unit mass when

used as fuel. The problem, however, is that although hydrogen is the most abundant element but is not available in free form and has to be produced from water or natural gas. Hydrogen production cannot be carried out in situ and thus hydrogen storage is necessary. It is the most challenging task as hydrogen has low density and boiling point. For increasing density, hydrogen can either be compressed to high pressures, liquefied at cryogenic temperatures or stored as a solid in metal hydrides.

Out of all the hydrogen storage methods, metal hydrides are particularly important because they provide a safe and convenient way to store hydrogen. The reason being they offer high volumetric hydrogen storage densities at low hydrogen gas pressures and also metal hydrides for few transition metals (TM) can be formed even at room temperature. TM-based hydrogen-absorbing alloys find applications in the fields of backup power, materials handling (forklifts), marine or submarine, etc.

A further innovation into hydrogen storage is the metal hydride composites (MHC) with expanded natural graphite (ENG). These can be used as a better alternative to metal hydride powders because they offer higher thermal conductivity and reduced porosity. Herbeig et al. [10] carried out neutron imaging studies to compare the structural stability and spatial-temporal hydrogen concentration of a MHC with loose metal hydride powder under cyclic hydrogenation. The results indicated that reversible hydrogen storage can be efficiently done in MHCs as the thermal resistance between MHC and container wall is very less compared to the loose powder bed as the latter tears apart whilst dehydrogenation (refer Fig. 10.6).

Hybrid storage systems which combine high-pressure vessels capability with some alloy-based hydrogen storage materials that absorb hydrogen under elevated pressures are also being considered for solving the issue of hydrogen storage. The internal structure of the hydrogen storage tank determines the performance of the

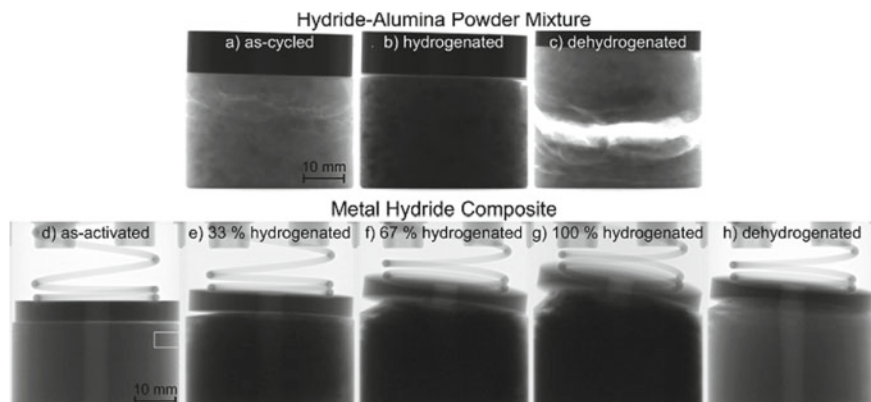
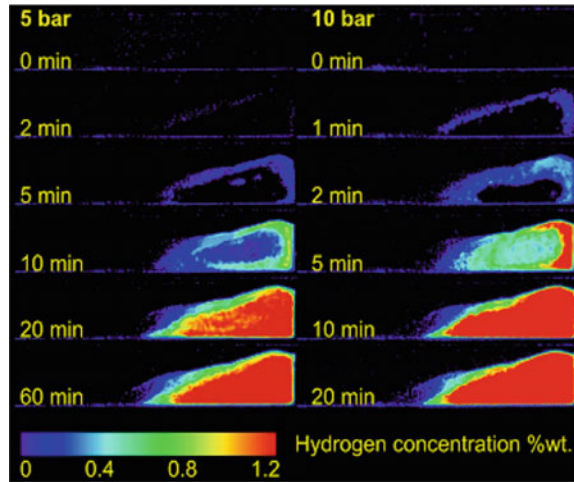


Fig. 10.6 a–c In situ neutron images during fast hydrogenation and fast dehydrogenation starting from the as-cycled state of a mixed hydride-alumina powder (HAP) sample. d–h In situ neutron images during slow (100 ml-H₂/min STP) hydrogenation and fast dehydrogenation (1st cycle) starting from the as-activated state [10]. Reproduced with permission from Elsevier Copyright Clearance Centre

Fig. 10.7 Neutron radiographs showing change in hydrogen concentration highlighting hydrogenating process kinetics at different pressures [11]. Reproduced with permission from Elsevier Copyright Clearance Centre



metal hydride or hybrid storage systems and studies have been carried out on different types of tanks available. Gondek [11] carried out neutron imaging studies on sodium alanate-based hydrogen storage tanks. Neutron radiography measurements were performed for the constant pressure conditions for the time predicted to be sufficient to obtain complete hydrogenation of the active material inside of the container. Radiographs were taken every minute, and results have been summarized as shown in Fig. 10.7. Figure 10.7 depicts the hydrogenation profiles under different pressures and time. It shows that the reaction speed increases by about three upon raising the pressure from 5 to 10 bar.

10.2.3 Neutron Imaging of Lithium-Ion Batteries

Energy storage has been a primary worldwide concern over the last few decades. Lithium-ion batteries (LIBs) with high energy densities are therefore the most sought of energy storage devices for microelectronic products. For meeting the requirements of large scale energy storage like smart grids and electric vehicles, there is a huge demand for producing high performance LIBs. LIBs are essentially electrochemical cells made of electrolytes and electrodes. To enhance their electrochemical performance, an understanding of the various components and processes along with degradation mechanisms of LIBs are important. In recent years, various techniques based on X-ray, electrons and neutron probes have been used to understand the mechanism of LIBs. Usage of neutrons provides complimentary data to X-ray and neutrons being chargeless are offer more penetrability thus are suitable for in situ studies even for commercial LIBs.

Owejan [12] used neutron imaging to get the lithium-ion distribution for an electrochemical cell. The cell used composite graphite as the negative electrode and

it was observed that the Li distribution in graphite was dependent on the state of charge. Zhang et al. [13] used neutron tomography to map the Li-ion spatial distribution in a V_2O_5 electrode of a small coin size cell. Imaging contrast between lithiated/delithiated states of V_2O_5 electrodes was sufficient to study the Li-ion distribution. Figure 10.8 shows the lithium distribution in a V_2O_5 cell obtained using

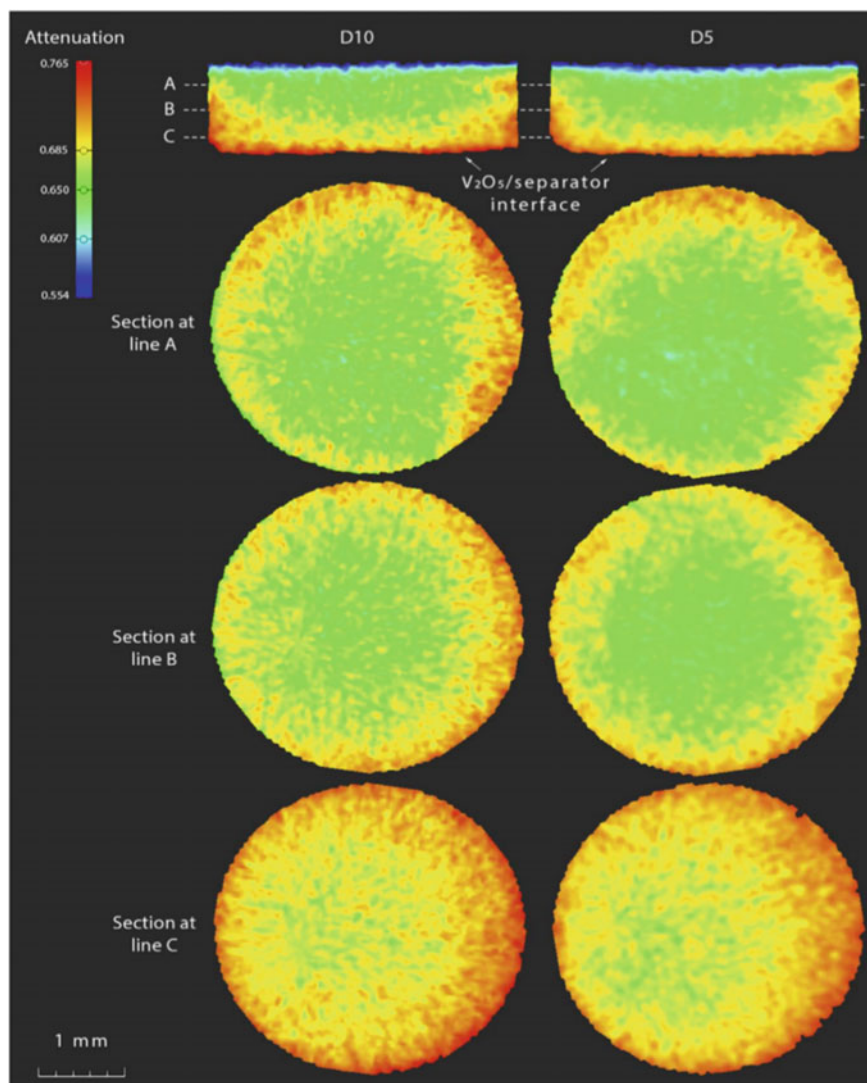


Fig. 10.8 Neutron imaging data showing lithium distribution in V_2O_5 electrode. In this pseudo-colour plot, higher attenuation represents higher Li concentration [13]. Reproduced with permission from Elsevier Copyright Clearance Centre

neutron tomography. It was observed that the Li spatial distribution is non-uniform within the bulk V₂O₅ cathodes. The non-uniformity is higher in the electrode where lithiation occurred relatively faster during the discharge (lithiation) [13].

Neutron imaging is an efficient probe for understanding the electrochemical processes inside the electrode. Understanding this can help in improving the batteries' performance both in terms of economic and safety reasons. To study the growth mechanism of lithium dendrite, Song et al. [14] used in operando neutron imaging. Figure 10.9 shows the basic set up used for the same and also the radiography and tomography results. The study helped in provide mechanistic insights with a deep understanding of dendrite Li shorting and redistribution. The information gained can be used for designing safer lithium electrodes. Thermal runaway of LIBs is an issue and the reason for the same is being explored. There are evidences that the thermal runaway begins with the decomposition of the solid electrolyte interphase (SEI) which is passivation layer formed on the electrodes during the first few charging cycles. Once the SEI is decomposed, the electrolyte reacts with electrode materials generating a large amount of heat and thereby exploding the LIBs. For developing safer LIBs, it is important to study the thermochemical stability of electrolyte and its wetting ability. Most electrolytes contain elements like C, H, O and therefore neutrons can serve as an excellent tool for their study.

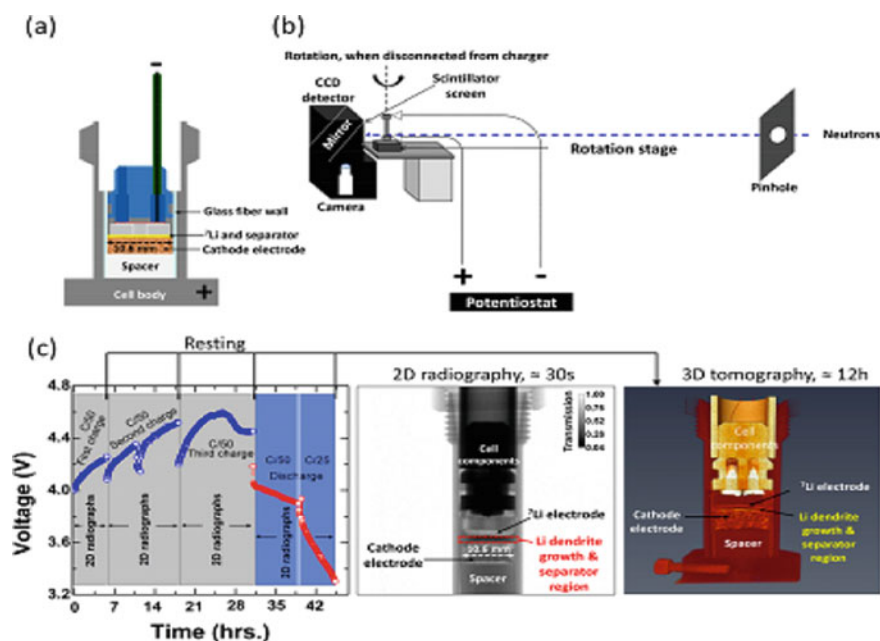


Fig. 10.9 a Electrochemical cell, b instrument setup at the beamline for the neutron radiography and tomography measurements and c charging/discharging profiles of the Li-ion battery during the experiment, highlighting the measurement strategy used for the radiography/tomography (open access)

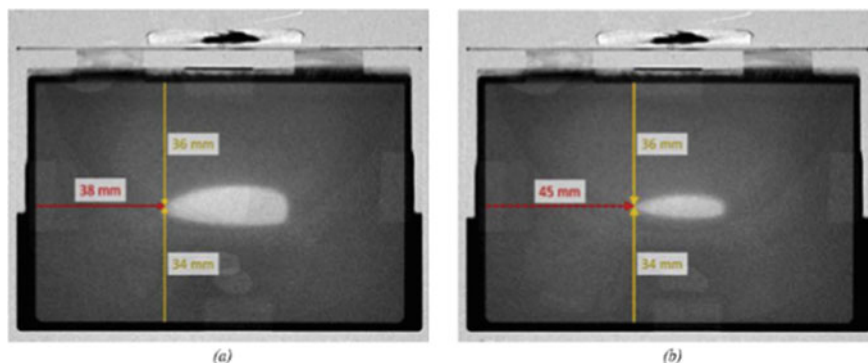


Fig. 10.10 Neutron radiograph of cell filled at vacuum shown **a** 33 min and **b** 41 min after the electrolyte filling [15]. Reproduced with permission from Elsevier Copyright Clearance Centre

The first application to electrolyte filling in LIBs visualization using neutron imaging was done by Weynadz [15]. Figure 10.10 shows the neutron radiographs of electrolyte filling in a cell at various instants.

Gases are released in LIB as a result of electrolyte decomposition and lead to the degradation of cells. In situ and in operando experiments are conducted to map the gas release behaviour of electrolyte-based batteries. Since the gases released are mostly light elements, neutron radiography can be used for the online studies. In situ neutron imaging studies have been used to observe the outgassing phenomenon in LIBs by Michalak [16]. Figure 10.11 shows the gassing caused by oxidation and reduction of the electrolyte solvent. It was inferred that the metal dissolution in the electrolyte and decomposition products formed as a result of high potential adversely affect the gas generation. This effect is most predominant in the first charge cycle when the SEI layer is getting formed.



Fig. 10.11 Neutron transmission images of a pouch cell illustrating the different processing steps. **a** After noise reduction, **b** after normalization to the first image and **c** after segmentation, with grey areas representing the generated gas [16] (open access)

10.2.4 Neutron Imaging for Crystalline Materials

Polycrystalline metallic alloys are used for structural support and related engineering applications. Understanding their microstructural properties and state of stress in various loading conditions is of immense importance towards their structural integrity and suitability for the required purposes. The available techniques for such investigations like metallography, electron microscopy and diffraction techniques are towards the surface or near-surface features and require sample preparation. Neutron diffraction has been the mainstay for crystal structure-related information for a long time rather than neutron-based imaging on account of the unavailability of imaging detectors having superior spatial and time resolving capability. Recent developments in transmission-based Bragg-edge imaging which is based upon the recording of transmitted intensity as a function of wavelength have shown promising results in providing scattering information in addition to the transmission image. With the introduction of these new advancements and also better detectors, neutron imaging now is being used as an efficient tool for characterizing crystalline materials.

Welding is an important process in almost every engineering component manufacture. When two dissimilar metals are weld, the weld quality is responsible for the structural integrity of the components. Since strain is developed in the process of welding, evaluation of the residual strain can be used to quantify the weld quality. Residual strain can be characterized by the microstructural features as well as element compositional distribution at the weld location.

Tremsin et al. [17] have reported such studies on Al-steel weld and Ti-steel butt weld with Cu as filler alloy through Time of flight (TOF) technique at the NOBORU beamline of material and experimental facility (MLF) of the J-PARC (Fig. 10.12). Crystallographic phase mapping by Bragg-edge imaging and elemental composition including intermetallic compound formation at the weld has been demonstrated. Nikolay et al. [18] have utilized the comparable lattice spacing length with the cold neutron wavelength to perform wavelength dependent transmission imaging using the time of flight technique with the help of energy resolving detector on weld joint between two austenitic plates. Wavelength dependent attenuation coefficient can be used towards deciphering information related to the microstructure of the specimen and Bragg-edge for its qualitative and quantitative phase composition analysis.

Using energy selective neutron tomography, Robin Woracek and his group [19] have carried out an interesting study on 3D mapping of crystallographic phase distribution in metastable 304 L stainless steel. The study, carried out on five samples, has revealed strain-induced phase transformation from austenite to martensite when subjected to tensile and torsional deformation beyond a certain plastic strain (Fig. 10.13). The transmission imaging results were verified by complimentary neutron diffraction studies. This technique has potential applications for the characterization of natural and advanced materials.

Austempered ductile iron (ADI) is a form of ductile iron that enjoys high strength and ductility as a result of its microstructure controlled through heat treatment. It

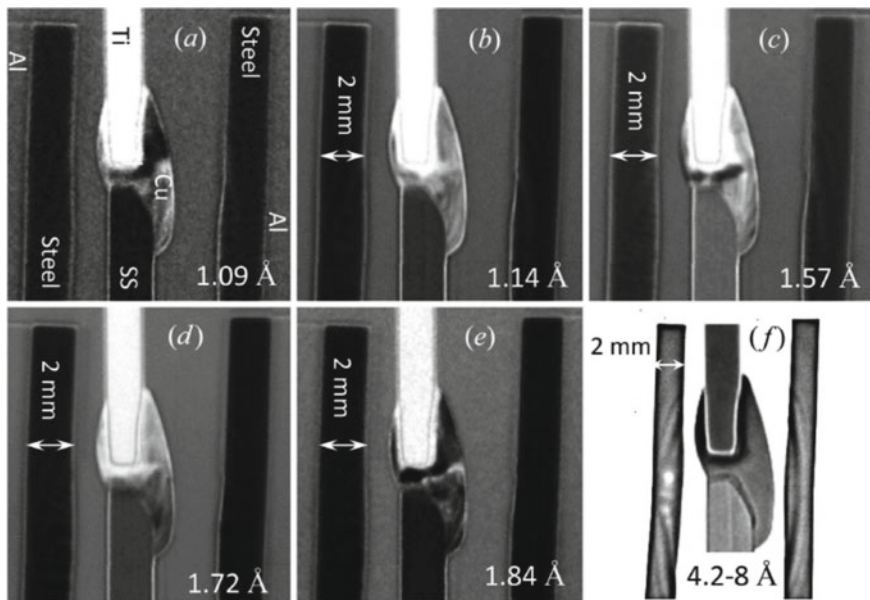


Fig. 10.12 Wavelength dispersive neutron transmission images of weld samples at Bragg-edges of steel and copper [17] (open access)

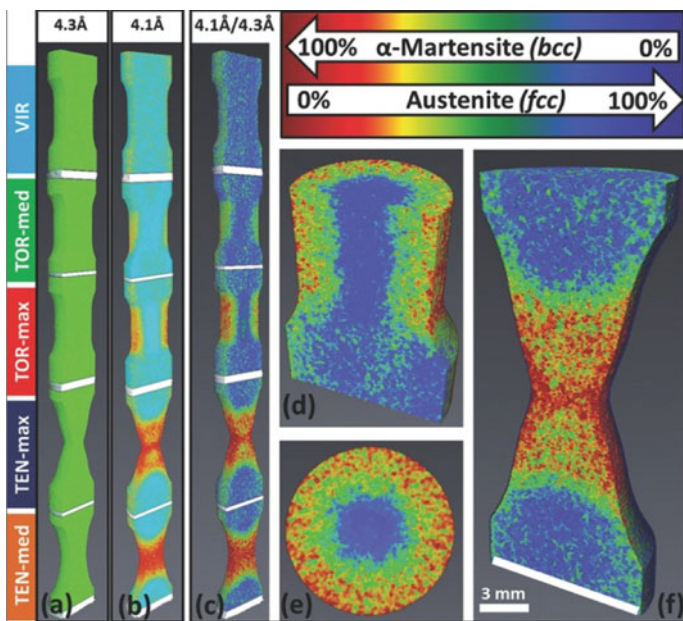


Fig. 10.13 Tomographic reconstruction of martensite and austenite phase fractions in 304 L stainless steel by using simultaneous neutron tomography at wavelengths before (4.1 Å) and after (4.3 Å) the ‘Bragg cut-off’ corresponding to the austenitic phase [19] (open access)

is a potential candidate to replace cast steel owing to its lighter weight, higher-tensile strength and significantly lower manufacturing cost. ADI is characterized by its spheroidal graphite nodules spaced within the matrix. These nodules reduce microsegregation of solutes within the material. For ADI, the material has been austempered such that the matrix is transformed into ausferrite, or a mixture of acicular ferrite and austenite. Soria et al. [20] investigated the spatial distribution of martensite content in ADI samples under different strain conditions using energy selective neutron radiography. Figures 10.14 and 10.15 show results for this study using two approaches. The first approach included taking images in the wavelength interval 1.6–5.9 Å, whilst for the second approach, only two specific wavelengths were chosen for imaging. For the first method, the martensite content was calculated

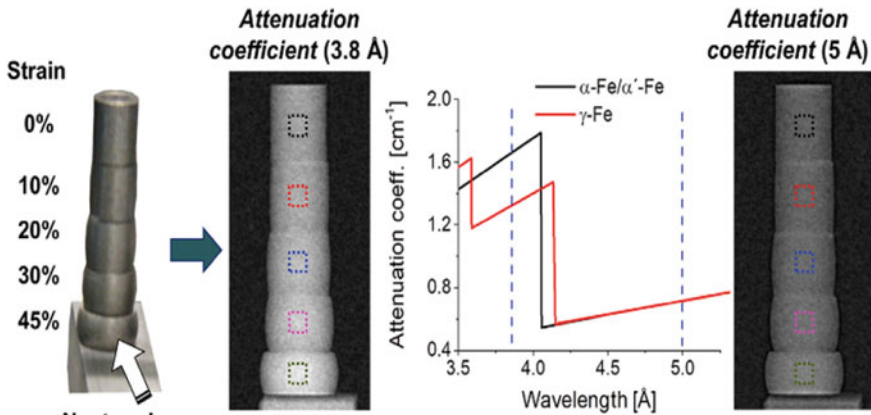


Fig. 10.14 Experimental setup of energy selective neutron radiography along with graph depicting the evolution of theoretical attenuation coefficient with change in wavelength. The change in Bragg-edge is clearly visible in the graph [20]. Reproduced with permission from Elsevier Copyright Clearance Centre

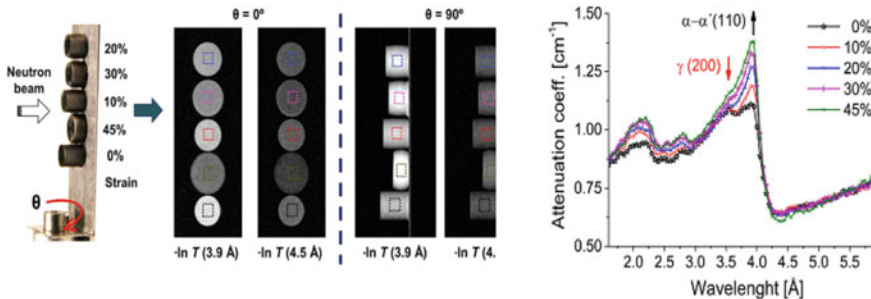


Fig. 10.15 (Left) Experimental setup of energy selective neutron radiography acquired at two wavelengths. (Right) Evolution of the experimental attenuation coefficient spectrum at different deformation level [20]. Reproduced with permission from Elsevier Copyright Clearance Centre

from the height of the selected Bragg-edge, whilst for the second one, the attenuation coefficient spectrum for different deformation levels provides the phase information.

10.3 Dynamic Neutron Imaging for Engineering Applications

Neutron radiography was first widely used in industrial applications in the mid-1950s. But these could only provide images of static samples. For real-time or near real-time events such as flow pattern studies, initial attempts were made using a modified version of medical fluoroscopy system based on image intensifier tube by Haskins [21], Bracher and Garret [22] and Stewart [23]. Berger [24] was the first to demonstrate real-time neutron radiography. Lindsay [25], in 1978, assembled and demonstrated the first successful neutron radiography facility at the United States University, University of Missouri, Columbia. The system comprised of a NE426, Li6F/ZnS(Ag) and Trimax, GdO2S , scintillator screens and ISIT camera. Later on with the advent of CCD cameras, imaging systems were developed by coupling them using lens and mirror to the converter screen. The mirror approach was necessary because the silicon imagers would otherwise be damaged by long-term exposure to neutrons and gammas. By the mid-1980s, improvements in digital imaging technology and the availability of advanced computers and image processing softwares enabled neutron radiography or radiography community to perform dynamic imaging with better image quality. Cooled CCD-based imaging units are very commonly used nowadays because of their good resolution and low noise. Being costly and also sensitive to radiation, these are properly shielded using B4C and lead. Because of the specific attenuation property of neutrons, they are very much suited for real-time flow pattern studies involving hydrogenous fluids inside metallic clad materials. Lindsay et al. (1992) [26] and Brunner et al. (2002) [27] applied NR for studying internal combustion engines, fuel flow, etc. Takenake et al. (2002) [28] have used neutron radiography to visualize fuel cavitation in a nozzle of a diesel engine. Norris et al. (1996) [29] studied water deposition in aerogel by neutron radiography method. Umekawa et al. (1999) [30] reported visualization of large particle movement in fluidized bed, Furui et al. (2002) [31] studied segregation process in fluidized bed, Asano et al. (1999) [32] calculated quantitatively void fraction data in fluid flow patterns using near real-time neutron radiography technique. Sinha et al. (1999) [33] had demonstrated prototype experiments on two-phase flow in metallic pipes using NR. Lots of work related to real-time neutron radiography and their advancements have been carried out by Lehmann [34], Harris [35], Jasti [36].

With the advancement in technology of various components related to neutron imaging, real-time imaging which were not possible earlier is being carried out routinely. The advancement can be linked to the availability of high-yield neutron sources (spallation), better beam quality arrangements (cold neutrons and $L/D \sim 500$

or more), sensitive as well efficient area detectors and high-end computing power. Real-time imaging with neutron is termed as neutron radioscopy.

10.3.1 Two-phase Flow Studies in Air–water Systems

Thermal hydraulics is an important part of various applications including heat transfer using fluids, immiscible fluid mixing, oil industry, etc. Various flow pattern generating modules have been developed, simulating the actual conditions, with air/water/oil/steam and experiments have been carried out at neutron imaging facilities. Since the flow is dynamic and to have the best result, one needs to capture every moment of the flow pattern. The source intensity, flow speed and the detector sensitivity play inter-dependent and cumulative role in deciding what studies to be carried out at which facility. In case of flow of gas and liquid in a vertical pipe, the liquid and gas phases distribute themselves into several recognizable flow structures. These are described below in brief:

- Bubbly flow—numerous bubbles dispersed in the continuous liquid phase.
- Slug flow—Bigger size bubbles forming specific shapes after coalescing several bubbles. This happens with increasing void fraction.
- Churn flow—With increase in flow speed oscillator motion sets in with net upward flow. This is an unstable flow pattern and is generally avoided.
- Annular flow—In this type of flow, the liquid is expelled from the centre of the flow as a thin film on the wall. There is a clear interface between the high velocity gas and liquid. This pattern is stable and is desired in two-phase flows. In this case, liquid droplets may get entrained in the gas.
- Wispy annular flow—This is formed at higher flow rates when the entrained droplets coalesce and forms cloud like coherent structures in the central vapour core.
- Mist flow—This flow happens at very high flow rates. The annular thin film gets sheared by the gas until it becomes unstable and is destroyed. This is inverse to what happens in the case of bubbly flow.

Since thermal neutrons are attenuated strongly by hydrogenous compounds such as water or oil, their flow inside metallic pipes, which are almost transparent to neutrons, can be visualized with contrast. Initial experimental work on two-phase (air-water) systems can be traced to the work of Mishima and co-workers [37–39] using Japan research reactor 3 M (JRR-3 M) of JAERI. The experimental conditions and components were as follows: thermal neutron flux was $\sim 10^8$ n/cm²/s, L/D was 153 (horizontal) and 176 (vertical), NE 426 scintillator coupled to high speed (1000 fps) video camera system coupled with a compatible image intensifier. Two-phase flow experiments were carried out in aluminium alloy made rectangular ducts. Images obtained from this experiment were processed to extract geometrical information to measure flow regime, velocity of bubbles, wave height, etc., as well as to measure the void profile and the average void fraction.

Advanced heavy water reactor (AHWR) is being developed in India for large scale thorium utilization in the third stage of Indian nuclear power programme. One of the passive safety aspects of this reactor is natural circulation-based heat removal using water. So the flow pattern and their transitions will govern the heat removal from the fuel. In other words, the study of flow pattern transitions can provide insights into the responsible operating parameters causing them. As for example, heat transfer from the fuel to the coolant is maximum in case of whole of the coolant pipe's internal volume is filled with water. But on account of heat, boiling occurs and hence various flow patterns set in such as slug, bubbly, annular and churn. This creates irregular heat transfer and disturbs the efficiency of the system. To perform hydraulic modelling and subsequent design of such a system, two-phase flow visualization for all possible scenarios is a must as such data are not available. A test setup involving a simulated loop made up of stainless steel pipe containing de-mineralized water with operating pressure range 1–70 bar was established at the old APSARA reactor (400 KW swimming pool type reactor which has been decommissioned) in BARC, India. The heating was carried out by a 10 kW heater at the portion that was radiographed. $^6\text{LiF-ZnS(Ag)}$ scintillator (NE 426) coupled to cooled intensified CCD camera was the imaging system used for this purpose. The imaging system was shielded with 150 mm thick concrete blocks to reduce background noise in the images. The radiography facility provided thermal neutron flux $\sim 10^6$ n/cm²/s at an L/D of 90 and cadmium ratio 6.3. Different case scenarios were generated by changing heating and water flow rate conditions [40, 41]. The configuration of the facility and imaging system along with storage processing provided 15 frame per second acquisition. Acquired data were processed using exponential and equally weighted schemes and void fraction were calculated for each frame and plotted against the process parameters. Experiments were conducted using 3/8" and 1/2" test sections. Though stable flow could be observed in 1/2" pipe, it was not the case for 3/8" pipe. This had been confirmed using in-house developed codes. Details of the Fig. 10.16 are as follows; (a) schematic of the APSARA reactor with test loop, (b) schematic of the test loop, (c) the imaging system, (d) typical frames showing the water flow in pipes (black represents water and white represents steam/air), (e) the instantaneous void fraction as seen on the monitor screen along with the averaged data followed, (f) exponentially weighted average and (g) equally weighted average plot. Prior to performing actual test loop experiment, feasibility experiments involving compressed air and water flow using neutron radiography were carried out.

Similar study involving air-water two-phase flow test loop has also been carried out at the thermal neutron beam port of IEN/CNEN Argonauta reactor, Rio de Janeiro [42]. The imaging conditions and system were as follows: thermal neutron flux at the exit of the port was 4.46×10^6 n/cm²/s, L/D:70, NE425 scintillator coupled to CCD-based video camera well shielded by borated paraffin, cadmium and lead. Different flow conditions were generated using a water pump and an air compressor in 6 mm diameter aluminium pipe. The studies carried out were drift flux correlation with different velocities of total two-phase flow and the void fraction.

The cases described above had the gas-liquid flow from bottom to top, i.e. in the upward direction. To understand the dynamics of flow towards efficient heat

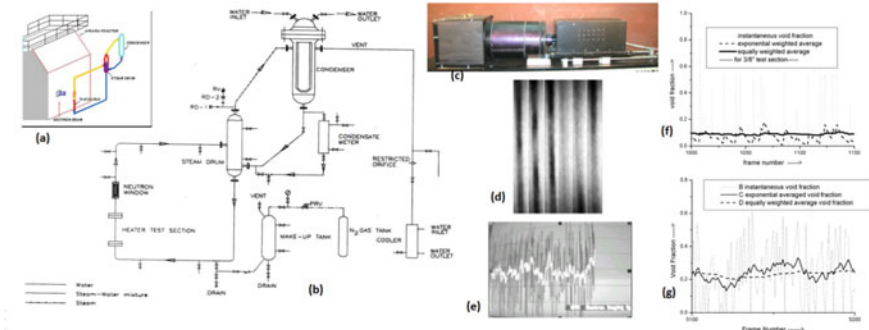


Fig. 10.16 **a** Schematic of the APSARA reactor with test loop, **b** schematic of the test loop, **c** the imaging system, **d** typical frames showing the water flow in pipes (black represents water and white represents steam/air), **e** the instantaneous void fraction as seen on the monitor screen along with the averaged data followed, **f** exponentially weighted average and **g** equally weighted average plot. Reproduced from [40] with permission from RightsLink by CCC

extraction in plate type heat exchangers Hitoshi Asano and co-workers [43] at Kobe University, Japan had carried out real-time neutron radiography towards visualization and void fraction distribution in plate type heat exchanger having downward gas-liquid two-phase flow. Experiments were carried out in the JRR-3 M neutron radiography facility at Japan Atomic Energy Research Institute (JAERI). Differences in flow characteristics between downward and upward flow were observed at low gas velocity conditions. It was also pointed out that liquid distribution into multiple channels strongly depended on the liquid volumetric flux.

10.3.2 Two-phase Flow Studies in Oil-Water Systems

Though heavy oil accounts for two-thirds of the world oil resources, on account of its high viscosity and presence of heavy distillates, its production is poor. In order to reduce oil viscosity, steam injection has been widely used but this has drawbacks such as severe carbon loss to coking causes low recovery efficiency and high energy consumption. In this regard, supercritical water injection technique for heavy oil recovery has been found to be beneficial as it not only reduces oil viscosity but also dissolves heavy distillates to avoid coking [44]. Shoji E and co-workers [45] have reported neutron radiography-based visualization studies regarding behaviour of heavy oil in supercritical water to understand the flow and mixing behaviour towards improving process efficiency related to supercritical water upgrading of heavy oil. M, Balasko and co-workers [46] at the Budapest Neutron Centre, Hungary have employed NR towards visualization and understanding of the segregation process in a closed loop liquid-liquid two-phase mixture involving 3-methylpyridine and heavy water with varying temperature and heavy water concentration. The images

in combination with analysis provided insights for development of models towards this type of flow patterns.

10.3.3 Two-phase Flow Studies in Liquid-Solid Systems

In the area of liquid—metal two-phase flow studies, real-time neutron radiography experiments carried out at the JRR-3 M thermal neutron radiography facility in the Japan Atomic Energy Research Institute (JAERI) using lead—bismuth eutectic as a working fluid and gold—cadmium intermetallic compound (AuCd_3) as tracer has been reported by Takenaka et al. [47]. Towards performing safety analyzes and understanding of severe accident in nuclear reactors, neutron radiography has always helped by providing real-time visualization and measurements in various experimental situations. Some notable scenarios are as follows: (a) steam explosion due to direct contact of molten metal and sub-cooled water simulating a severe accident of a light water reactor and (b) gas-molten metal mixture in a pool simulating a severe accident of a fast breeder reactor. Mishima et al. [48] have reviewed important aspects related to application of neutron radiography to thermal hydraulics research. Neutron radioscopy technique has been efficiently utilized for basic understanding of liquid—metal two-phase flow visualization and measurements [49] of nitrogen gas—molten lead bismuth two-phase flow in respect to fast reactor research.

In the area of power production using advanced fourth generation reactors, fast breeder reactors offer the opportunity towards effective use (60–70%) of natural uranium resources [50]. Since the cores of fast reactors are compact, huge amount of heat removal is necessary. Liquid metals offer the best solution in such cases. So, understanding the heat transfer mechanism along with the flow characteristics, neutron radiography-based real-time imaging is being carried out across the globe. These sorts of studies are a necessary prerequisite not only for safety analysis of liquid-metal fast breeder reactors (LMFBRs) but also for the development of liquid-metal magneto-hydro-dynamics (MHD) system. High frame-rate neutron radiography of liquid metal two-phase flows in metallic vessels was studied by Saito et al. [51] towards understanding of gas—liquid metal flow characteristics.

10.3.4 Lead Melting and Solidification Studies

As per performance standards specified by IAEA, AERB in India, radioactive materials are transported in steel shells canisters inside lead shielded packages. The design of packaging of nuclear materials for such cases is aimed towards their safety, taking into considerations of all accident scenarios (example fire) such that there should not be any streaming of radiation. Lead casks are subjected to open pool fire test at 800 °C for 30 min amongst other tests to ascertain their performance stability. Study of lead melting towards designing transportation packages for radioactive materials

is very important for estimating their performance. Experimental data in such cases are required for the development of benchmarking with high confidence. Numerical modelling becomes impossible when inaccuracies due to strong non-linearity of the governing equations combined with a moving boundary, created by the heating mechanism, sets in. During the melting process, solid-liquid phase transition takes place and the flow patterns are governed by the temperature, heating mechanism and the flow velocity. Knowledge of these parameters is of utmost importance to carry modelling. Thermocouple probe-based techniques have been used by lot of researchers (Emrich 1981) for recording the temperature at various locations in the bulk and get information of the melting or solidifying front with respect to time. Disadvantages with this technique are that they disturb the molten propagating front as they are embedded inside the bulk and also they provide information at a particular point. Basically, this technique is of intrusive type. A number of studies towards melting have been reported by F Wolf and R. Viskanta for tin [52] and by C Beckermann and R Viskanta for gallium [53]. Ultrasound wave-based imaging has been proved to be a promising tool for getting temperature information (Sielschott 1997; Xu et al. 2002). Ultrasound thermometry-based laboratory experiments have been carried by Fife et al. [54] for optical and opaque metallic fluids for understanding of the convection flow patterns. Various techniques towards obtaining temperature profiles at boundaries of the test specimens for understanding the flow pattern transitions have also been employed. These are flow velocity measurements using hot wire anemometry, laser Doppler anemometry or ultra sound anemometry, infra-red thermography (Carlomagno 1993).

All the techniques mentioned above are somewhat indirect in nature towards interpretation of the melting or solidification phenomena related to the process parameters. None provided direct images signifying distinct regions in terms of solid and its molten counterpart. Projection-based radiography technique has the ability to provide two dimensional images with clear demarcation of the solid-liquid phase. For light elements, X-rays can be employed as probes. Observation of melt-solid interfaces, their shape and movement in germanium and lead tin telluride crystals during their growth has been reported by Yin et al. [55], Barber et al. [56] using X-rays. On a similar manner, gamma ray tomography-based studies have been carried out by Chun et al. [57] for online monitoring of solidification front in metal castings. But, X-ray or gamma ray imaging fails for thick and high Z materials such as lead. Neutrons come to the rescue in such cases as they have the unique property of getting highly attenuated by materials such as hydrogen, water, boron, gadolinium and cadmium and much lesser for materials such as aluminium, iron and lead. Though neutron radiography has been used as non-destructive technique for various studies such as flow pattern transition in water-air mixture inside metallic pipes, oil flow inside motor engines [58–61], water ingress in concrete [62] and metallic composite structures [63], there has been limited study on lead melting and solidification process and their interface propagation using it. Some research work in the domain of solid melt studies using NR are Pb-Bi specimens by Takenake et al. [64] and Ogino et al. [65] employing tracer induced and dye injection methods and observation of segregation in Sn-Cd alloy metals by Reijonen et al. [66].

Feasibility experiments on imaging of solid-liquid interface of lead melting and solidification phenomena using non-invasive NR technique have been carried out at neutron imaging beamline, CIRUS reactor (at present decommissioned), India for visualization of the interface during both melting and solidification process and understand the convection driven phenomena with respect to time and heating power.

The neutron imaging beam line characteristics were as follows: $L/D \sim 125$, bismuth plug at the collimator inlet to reduce gamma background, flux at sample position $\sim 3 \times 10^6$ neutrons /sec. The neutron imaging system consisted of ${}^6\text{LiF-ZnS}$ converter screen, a front coated aluminium glass mirror and a cooled CCD camera (1250 \times 1050 pixels, pixel size 22 μm , Model: DW432N) and provided resolution $\approx 100 \mu\text{m}$. For the safety of the CCD camera, it was shielded using lead and borated polythene blocks. The schematic of the imaging system is shown in Fig. 10.17a and the actual photograph of the installed imaging system in Fig. 10.17b.

50 mm cube Pb block (99.9%) was heated from one side using heating coil. Attached thermocouples provided the temperature details. To ascertain the contrast sensitivity across the Pb block, small Pb sheets of thickness 1.5 mm and 3 mm were placed behind it and imaged. They provided 7% and 15% contrast with respect to the Pb block which amounted to a density difference of 3% and 5.6%, respectively. This was better than the required condition of 6% contrast which is the case for 50 mm solid and liquid Pb. Real-time neutron radiography was carried out at heating powers of 150 W, 175 W and 200 W with the individual exposure of 10 s and frame to frame time difference of 3.8 s. This was optimized with experiments to provide sufficient contrast in the images towards visualization and quantitative analysis. Figure 10.18 shows the lead melting front shape and position at different time instances for three heating powers. These experiments provided data related to modelling and benchmarking [67]. In a similar way, solidifications of the molten lead were also carried out for all the heating conditions by putting OFF the heater at the completion of melting phenomena. Typical images during the solidification are shown in Fig. 10.19. Also

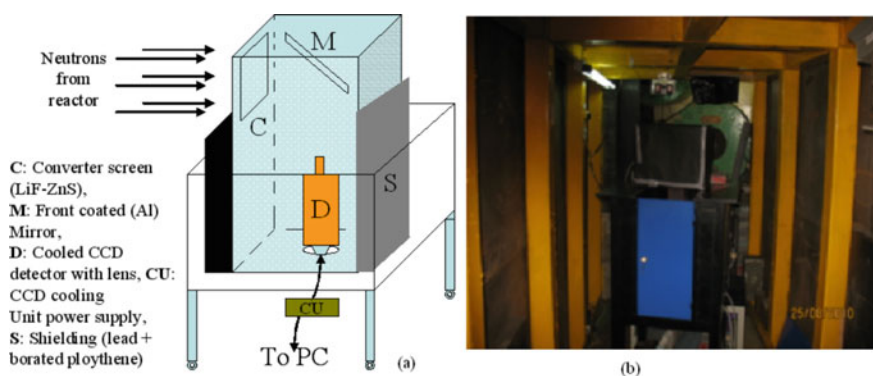


Fig. 10.17 a Schematics of the imaging system along with its components and b the actual photograph of the imaging system as installed at e-12 beamline, CIRUS Reactor, India. The imaging box is on top of the blue coloured table [68]

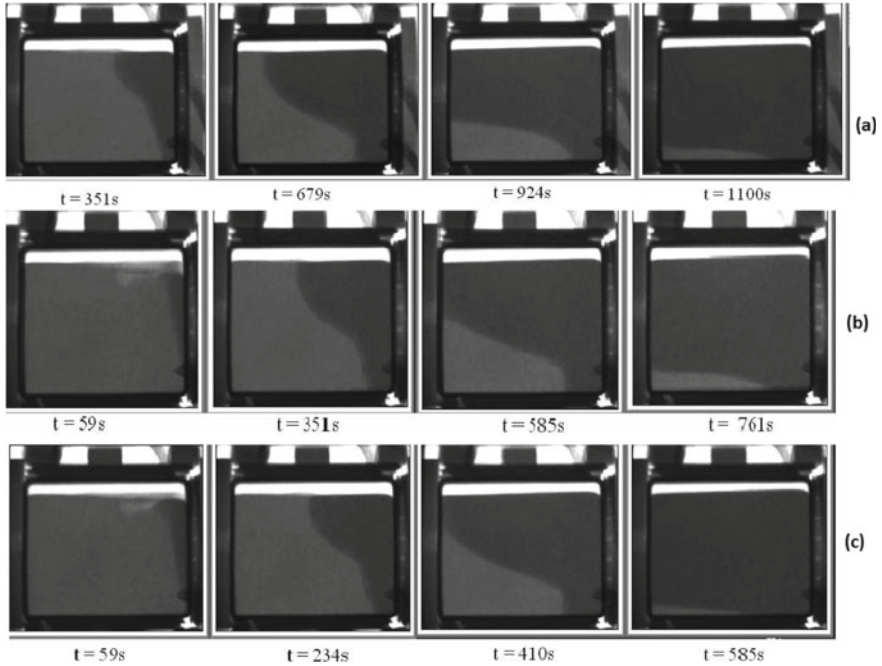


Fig. 10.18 Typical neutron radiography images clearly showing the propagation of melting front at various instances for heating powers, **a** 150 W, **b** 175 W and **c** 200 W

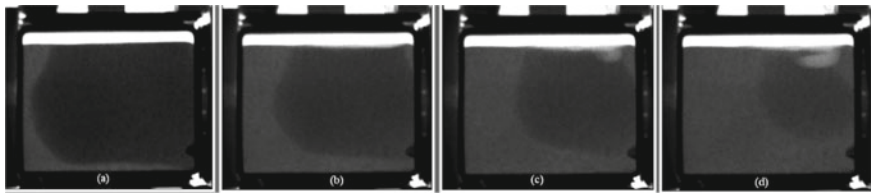


Fig. 10.19 Neutron radiography images of solidifying front propagation at four instants of time

when the study was carried out using impure lead, a separate mushy region was also visualized. Details of the experiment at result are provided in [68].

Using pulsed neutron transmission spectroscopy and nGEM as detector, visualization of solidification phases of lead bismuth eutectic in the energy resolved pulsed neutron imaging beamline at BL22, RADEN facility in J-PARC has been carried out [69]. LBE is under study for its excellent characteristics towards its use as coolant in accelerator driven systems. The radiographs and Bragg-edge images provided transient data during solidification for better understanding through numerical modelling.

10.3.5 Dynamic Imaging of Combustion Engine

Since thermal neutron is sensitive to hydrogen like elements, study of fuel (hydrocarbon-based) behaviour such as calibration or flow in a diesel engine or nozzle design efficiency are possible using neutron as probe. These are important related to fuel injection in diesel engine towards increasing the system efficiency. Cavitation process hampers the supply of fuel to the engine. This sort of study has been reported by Takenaka and co-workers [70, 71] at JAERI, KAERI and Kyoto University Research (KUR) reactor facility. Various configurations such as one injection hole and four injection holes in a nozzle for a truck, a nozzle for a ship and a nozzle for a dynamo were studied for exposure time ranging from 4 to 120 s using cooled CCD camera system utilizing LiF-ZnS(Ag) screen as neutron convertor. Typical images of gas bubbles in the nozzle are shown in Fig. 10.20. Synchronization of the motor with imaging system was carried out through chopper. Owing to this, the signal to noise ratio was poor as neutron flux to the sample was limited.

With the advent of spallation neutron sources, high yield of thermal neutron flux as well as in pulsed mode was possible. Researchers at TUM, Berlin and PSI, SINQ, NEUTRA Switzerland have carried out dynamic radiography of a 125 cc four stroke Yamaha make motorcycle engine using spallation source SINQ at PSI [72]. Synchronized images at various positions of the piston were acquired at source strength $\sim 7 \times 10^6$ n/cm²/s and L/D 350. The imaging system comprised of ⁶Li loaded neutron scintillator and image intensifier coupled CCD camera images (exposure 0.1 ms) at different rotation speeds up to 1200 rpm were taken and averaged images provided crucial information regarding fuel flow in the running engine.

Similar work on short time stroboscopic neutron imaging and measurement on a rotating engine has been carried out at ILL, Grenoble [73] which is one of the most intense continuous neutron flux in the world. They have examined an electrically driven BMW engine, operated at 1000 rpm with the resolution of 200 μ s. For this short time imaging, multichannel plate-based intensified CCD camera, capable of

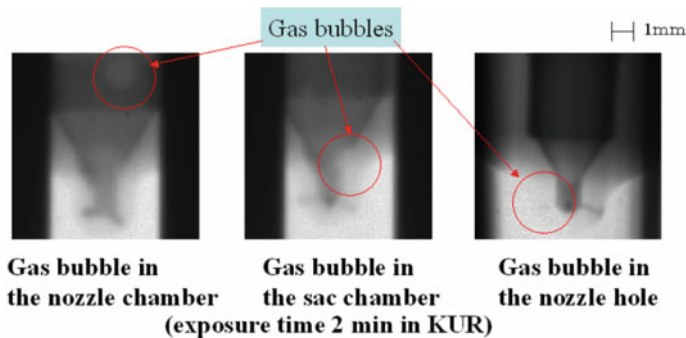


Fig. 10.20 Visualization of gas bubbles in the nozzles using real-time neutron radiography at the KUR. Reproduced from [71] with permission from RightsLink by CCC

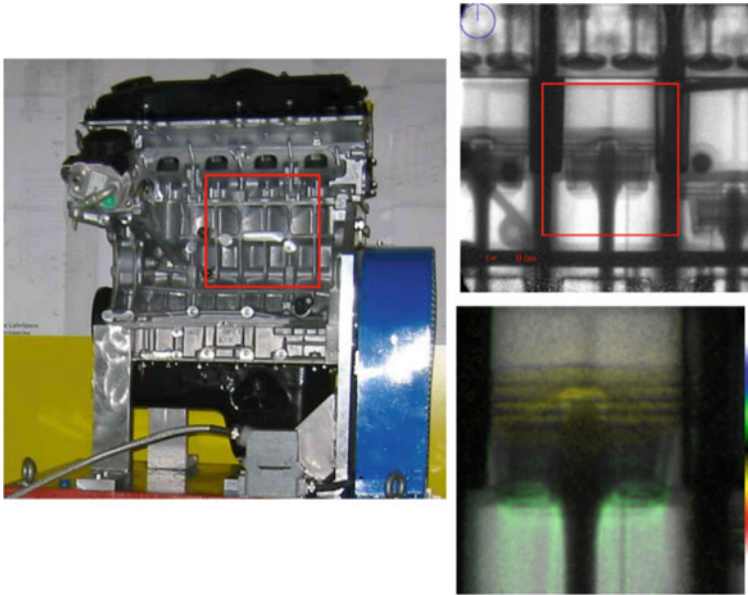


Fig. 10.21 (Left) Photograph of the BMW combustion engine, the field of view for neutron radiography is marked by red rectangle, (right top) a typical NR frame of the running engine and (right bottom) overlapped images, with pseudo colouring, revealing the oil inside the engine. Reproduced from [73] with permission from Author

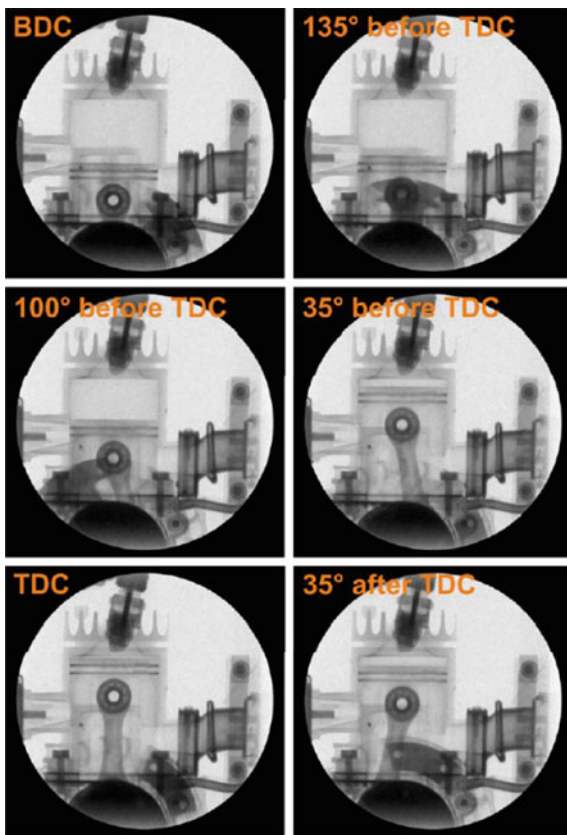
triggered imaging, was used. Photograph of the BMW combustion engine, a typical NR frame of the running engine and overlapped images, with pseudo colouring, revealing the oil inside the engine is shown in Fig. 10.21.

On the same line of work, PSI researchers have imaged in real time the moving part of a two-stroke chain saw engine running at idle speed (~ 3000 rpm) and at 8000 rpm, the combustion chamber and the crank shaft [74, 75]. Visualization of fuel and lubricants distributor inside the cylinder in real-time condition was possible. Owing to high flux from spallation sources, image acquisition for short time $\sim 50 \mu\text{s}$ with a spatial resolution of $100 \mu\text{m}$ could be carried out (Fig. 10.22). To increase the contrast in the images, gadolinium oxide nanoparticles were dispersed in the fuel.

10.3.6 Neutron Imaging of Fluidized Bed

A fluidized bed is a process where mixing of solid particulate with fluid/gas takes place under appropriate conditions underlying the physical phenomenon of optimum mixing for process enhancement. This phenomenon, where the solid particles behave fluid-like, is known as fluidization. During the fluidization process, fluid drag force and particles gravitational force become equal and the solid particles become

Fig. 10.22 Dynamic neutron radiographs of the prepared two-stroke engine at different crank angle positions between the bottom dead centre (BDC) and the top dead centre (TDC). Reproduced from [74] with permission from RightsLink by CCC



suspended. Fluidized beds are advantageous for the conditions such as area of interaction increases as the particle size goes small which means increase in efficiency, gases/fluids can transfer heat and mass transfer at much higher rates as opposed to solids, operations can be controlled smoothly, rapid mixing enable isothermal conditions throughout the mixing volume can be scaled up, small surface requirement for heat exchangers within the fluidized bed and so on. Though there are some disadvantages, such as very short duration residence time of solid particles for very high flow rate and erosion/abrasion in vessels, the advantages outweigh their use for various applications. Some commercial applications of fluidized bed involving solid/gas/liquid phases are combustion and incineration, roasting of ores, gasification, drying of particles, granulation, etc. To make the reader understand about the fluidized bed concept, let us take a simple example. In case of power generation by burning coal and coal based fuels, the efficiency is ~35 to 37%. Towards increasing the efficiency, formation of a gaseous mixture containing hydrogen and carbon monoxide generated by gasification of coal with air/oxygen and steam at high pressure is beneficial. Pressurized fluidized bed gasification is such a process which increases the coal efficiency to 45%.

To understand the process and the effect of process parameters, one needs to look inside the bed non-intrusively. If the vessel is made up of metal and has some thickness to be safe for high-pressure and high temperature conditions, optical and to some extent X-rays are of no help as they will be attenuated mostly by the clad material. In the case one uses high energy X-rays, there will be almost no contrast between the solid phase and the mixed phase due to very low attenuation in the bed material. Several works related to use of probe method have been cited but they are intrusive type and modifies the bed conditions to some extent. In such cases, neutrons are helpful as they can be used as non-intrusive probe and their attenuation to metals is very less and much higher with fluid/air. In case where mixing of two types of solid particulates are involved, providing one of them with neutron absorbing coating to generate higher neutron attenuation can be employed to obtain high contrast images. Some case studies in fluidized bed using real-time neutron radiography are discussed.

Initial work carried out by Catchen and his team [76] on development of neutron radiography technique for investigating physical models of fluidized bed has laid the way towards this domain of study. They have setup a 15 cm thick sand model and thin-walled aluminium shells simulating spherical voids as a fluidized bed. Experiments were carried out using image intensifier and convention photography techniques in a nuclear reactor beamline to understand various scenarios including dynamic condition.

Understanding of bed particle movement in a fluidized bed provides information about the various mechanisms and process parameters involved. Hisashi Umekawa and his team [77] at the Kansai University, Japan in collaboration with JAERI have carried out neutron radiography of simulated aluminium plate fluidized bed having sand as the bed material. Since both the materials are transparent to neutrons, sand particles were coated with CdSO_4 , which brought out the contrast. To visualize bulk bed movement, particles made up of B_4C (diameter ~ 2 mm) were used in the bed as tracer particles. The experiment proved with no doubt that tracer-based NR has high potential towards meaningful data in understand fluidized bed movement in such cases of bed material. Using GdSO_4 in place of CdSO_4 , similar experiments have also been carried out by S. Furui and group [78] towards understanding segregation process in fluidized bed involving binary mixture systems.

Theoretical modelling is a prerequisite in designing any combustion/reaction system based on fluidized bed concept. The relationship between the heat transfer, mixing process and/or diffusion of the reacting gas with bubble or void nature of the bed needs understanding. Real-time NR images with suitable image processing tools have also provided great deal of information regarding the bubble behaviour such as bubble size, bubble frequency, bubble trajectory in vertical tube-banks immersed in a bed [79]. Fluidized bed studies involving different particles have pointed out that segregation phenomena hampers the efficient combustion or reaction, say in a chemical plant. The segregation characteristics depend upon various factors including the particle size distribution, packing ratio and fluidizing gas velocity. Utilizing both X-ray and neutron radiography such experiments have been performed at JAERI [80].

10.4 Summary

This chapter has tried to provide a glimpse on some important applications of neutron imaging related to material science and engineering with the aim to study process parameter, process efficiency, new material development, etc. The know-how obtained through neutron imaging forms the basis for future capacity enhancement towards societal and economic development. To name a few, attenuation-based neutron imaging in the field of PEM-based fuel cell research, hydrogen storage materials, issues related to lithium distribution and thermal runaway in Li-ion batteries have yielded great deal of information towards maximizing their output. Study of material distribution at the weld juncture between two materials using wavelength dispersive imaging has enriched us with crystallographic phase mapping as well as elemental composition including intermetallic compound formation. With the advent of advanced and efficient neutron imagers coupled with the availability of intense sources, dynamic neutron imaging has proved an indispensable probe towards understanding of processes and its controlling parameters. Various flow conditions probed using neutron imaging technique in systems involving air-water, oil-water, liquid-solid, melting-solidification phenomena in lead, combustion engine, fluidized bed have been discussed. The outcome of these sort of experiments provides information related to the processes and helps in improving their utility in their intended applications.

References

1. Nsour W, Taa'mneh T, Ayadi O, Al Asfar J (2019) Design of stand-alone proton exchange membrane fuel cell hybrid system under Amman climate. *J Ecol Eng.* <https://doi.org/10.12911/22998993/111800>
2. Tötze C, Manke I, Hilger A, Choinka G, Kardjilov N, Arlt T, Markötter H, Schröder A, Wippermann K, Stolten D, Hartnig C, Krüger P, Kuhn R, Banhart J (2011) Large area high resolution neutron imaging detector for fuel cell research. *J Power Sources* 196:4631–4637
3. Markötter H, Manke I, Kuhn R, Arlt T, Kardjilov N, Hentschel MP, Kupsch A, Lange A, Hartnig C, Scholta J, Banhart J (2012) Neutron tomographic investigations of water distributions in polymer electrolyte membrane fuel cell stacks. *J Power Sources* 219:120–125
4. Stahl P, Biesdorf J, Boillat P, Kraft J, Friedrich KA (2015) Water distribution analysis in the outer perimeter region of technical PEFC based on neutron radiography. *J Electrochem Soc* 162(7):F677–F685
5. Manke I, Banhart J, Haibel A, Rack A, Zabler S, Kardjilov N, Hilger A, Melzer A, Riesemeier H (2007) In situ investigation of the discharge of alkaline Zn–MnO₂ batteries with synchrotron X-ray and neutron tomographies. *Appl Phys Lett* 90:214102 (Former removed)
6. Turhan A, Kim S, Hatzell M, Mench MM (2010) Impact of channel wall hydrophobicity on through-plane water distribution and flooding behavior in a polymer electrolyte fuel cell. *Electrochim Acta* 55:2734–2745
7. Biesdorf J, Forner-Cuenca A, Schmidt TJ, Boillat P (2015) Impact of hydrophobic coating on mass transport losses in PEFCs. *J Electrochem Soc* 162(10):F1243–F1252
8. Fairweather JD, Spornjak D, Weber AZ, Harvey D, Wessel S, Hussey DS, Jacobson DL, Artyushkova K, Mukundan R, Borup RL (2013) Effects of cathode corrosion on through-plane water transport in proton exchange membrane fuel cells. *J Electrochem Soc* 160(9):F980–F993

9. Katzel J, Markotter H, Arlta T, Klages M, Haubmann J, Messerschmidt M, Kardjilov N, Scholta J, Banhart J, Manke J (2016) Effect of ageing of gas diffusion layers on the water distribution in flow field channels of polymer electrolyte membrane fuel cells. *J Power Sources* 301:386–391
10. Herbrig K, Pohlmann C, Gondek L, Figiel H, Kardjilov N, Hilger A, Manke I, Banhart J, Kieback B, Rontzsch L (2015) Investigations of the structural stability of metal hydride composites by in-situ neutron imaging. *J Power Sources* 293:109–118
11. Gondek L, Selvaraj NB, Czub J, Figiel H, Chapelle D, Kardjilov N, Hilger A, Manke I (2011) Imaging of an operating $\text{LaNi}_{4.8}\text{Al}_{0.2}$ based hydrogen storage container. *Int J Hydrog Energy* 36:9751–9757
12. Owejan K, Gagliardo J, Harris S, Wang H, Hussey D, Jackson D (2012) Direct measurement of lithium transport in graphite electrodes using neutrons. *Electrochem Acta* 66:94–99
13. Zhang Y, Ravi Chandran KS, Bilheux HZ (2018) Imaging of the Li spatial distribution within V_2O_5 cathode in a coin cell by neutron computed tomography. *J Power Sources* 376:125–130
14. Song B, Dhiman I, Carothers JC, Veith GM, Liu J, Bilheux HZ, Huq A (2019) Dynamic lithium distribution upon dendrite growth and shorting revealed by operando neutron imaging. *ACS Energy Lett* 4:2402–2408
15. Weydanz WJ, Reisenweber H, Gottschalk A, Schulz M, Knoche T, Reinhart G, Masuch M, Franke J, Gilles R (2018) Visualization of electrolyte filling process and influence of vacuum during filling for hard case prismatic lithium ion cells by neutron imaging to optimize the production process. *J Power Sources* 380:126–134
16. Michalak B, Sommer H, Mannes D, Kaestner A, Brezesinski T, Janek J (2015) Gas evolution in operating lithium-ion batteries studied in situ by neutron imaging. *Sci Rep* 5:15627. <https://doi.org/10.1038/srep15627>
17. Trensins AS, Ganguly S, Meco SM, Pardal GR, Shinohara T, Bruce Feller W (2016) Investigation of metal welds by neutron imaging. *J Appl Cryst* 49:1130–1140
18. Kardjilov N, Manke I, Hilger A, Williams S, Strobl M, Woracek R, Boin M, Lehmann E, Penumadu D, Banhart J (2012) Neutron Bragg-edge mapping of weld seams. *Int J Mater Res* 103(2):151–154
19. Woracek R, Penumadu D, Kardjilov N, Hilger A, Boin M, Banhart J, Manke I (2014) 3D mapping of crystallographic phase distribution using energy-selective neutron tomography. *Adv Mater* 26(24):4069–4073
20. Soria SR, Li XH, Schulz M, Boin M, Hofmann M (2020) Determination of martensite content and mapping phase distribution on Austempered Ductile Iron using energy-selective neutron imaging. *Mater Charact* 166:110453
21. Haskins JJ (1973) Evaluation of a real time imaging system for Neutron Radiography. General Electric Report, NEDC 12512, 29 May 1973
22. Bracher DA, Garrett DA (1975) Abstract only. *Mater Eval* 33:47A
23. Stewart PAE (1975) Patent Specification 1 542 860, filed, 23 Dec 1975
24. Berger H (1966) Characteristics of a thermal neutron television imaging system. *Mater Eval* 24(9):475–481
25. Lindsay JT (1983) Development and characterization of a real time neutron radiographic imaging system. Ph.D. Dissertation, University of Missouri
26. Lindsay JT et al (1992) A summary of neutron radiography and its application to the study of internal combustion engines and fluid flow. In: Proceedings of the fourth world conference on neutron radiography, San Francisco, California, USA, 10–16 May 1992, pp 324–332
27. Brunner J, Lehmann E, Schillinger B (2002) Dynamic neutron radiography of a combustion engine. *Neutron Radiography* (7), Proceedings of the Seventh World Conference, Roma, Italy, 15–21 Sept 2002, pp 439–446
28. Takenaka N, Kadowaki T, Kawabata Y, Sim CM, Nam KY (2002) Towards the visualization of fuel cavitation in a nozzle of a diesel engine by neutron radiography. *Neutron Radiography* (7), Proceedings of the seventh world conference, Roma, Italy, 15–21 Sept 2002, pp 453–458
29. Norris PM, Brenizer JS, Raine DA, Bostain DA (1996) Measurement of water deposition in aerogel by neutron radioscapy. In: Fischer CO, Stade J, Bock W (eds) Fifth world conference on neutron radiography, proceedings, 17–20 June 1996, Berlin, Germany, pp 602–609

30. Umekawa H, Ozawa M, Onodera T, Okura Y, Takenaka N, Matsubayashi M (1999) Visualization of large-particle movement in fluidized-bed by neutron radiography. *Neutron Radiography* (6), Proceedings of the sixth world conference, Osaka, Japan, 12–21 May 1999, pp 507–514
31. Furui S, Umekawa H, Hayashi K, Ozawa M, Takenaka N (2002) Flow visualization of segregation process in a fluidized-bed by neutron radiography. *Neutron Radiography* (7), Proceedings of the seventh world conference, Roma, Italy, 15–21 Sept 2002, pp 431–438
32. Asano H, Takenaka N, Fujii T, Arakawa T, Matsubayashi M (1999) Quantitative measurement of void fraction distribution. *Neutron Radiography* (6), Proceedings of the sixth world conference, Osaka, Japan, 12–21 May 1999, pp 515–522
33. Sinha A, Vijyan PK, Shaikh AM (1999) Visualization and analysis of two phase flow by neutron radiography and its applications in the thermal hydraulics studies of advanced reactors. *Neutron Radiography* (6), Proceedings of the sixth world conference, Osaka, Japan, 12–21 May 1999, pp 545–554
34. Neutron Imaging, E. H. Lehmann (Department Spallation Neutron Source, Paul Scherrer Institute, CH-5232 Villigen PSI, Switzerland), *Neutron scattering in novel materials*, 22–36 Nov 2000
35. Harris DHC, Seymour WAJ (1987) Applications of real time neutron radiography at Harwell. In: Barton JP, Farny G, Person JL, Röttger H (eds) *Neutron radiography*. Springer, Dordrecht
36. Jasti JK, Fogler HS (1992) Application of neutron radiography to image flow phenomena in porous media. *AIChE J* 38:481–488
37. Mishima K, Fujine S, Yoneda K, Yonebayashi K, Kanda K, Nishihara H (1992). In: Jones OC, Michiyoshi I (eds) *A study of air-water flow in a narrow rectangular duct using an image processing technique, dynamics of two-phase flow*. CRC Press, Boca Raton, pp 141–160
38. Hibiki T, Mishima K, Yoneda K, Fujine S, Kanda K, Nishihara H, Tsuruno A, Matsubayashi M, Sobajima M, Ohtomo S (1994a) Proceedings 4th world conference neutron radiography, San Francisco, CA, 10–16 May, *Neutron Radiography*, 4th edn. J.P. Barton Gordon and Breach, Yverdon, Switzerland, p 317
39. Mishima T Hibiki K, Nishihara H (1997) Visualization and measurement of two-phase flow by using neutron radiography. *Nuclear Eng Des* 175(1–2):25–35
40. Sarkar PS, Kashyap Y, Sinha A, Vijyan PK, Prasada Rao GSS (2005) Applications for real-time neutron radiography for convection driven flow pattern transition studies. *IEEE Trans Nuclear Sci* 52(1)
41. Sinha A, Vijyan PK, Shaikh AM (1999) Visualization and analysis of two phase flow by neutron radiography and its applications in the thermal hydraulics studies of advanced reactors. Presented at the 6th world conference on neutron radiography held at Osaka, Japan, 17–21 May
42. Luiz LC, Crispim VR, Ferreira FJO (2010) Visualization of two-phase flow in metallic pipes using neutron radiographic technique. *Physica* 9:19–23
43. Hitoshi A, Nobuyuki T, Terushige F, Toshiaki W (2005) Visualization and void fraction distribution of downward gas-liquid two-phase flow in a plate heat exchanger by neutron radiography. *Nuclear Instrum Methods Phys Res Sect A: Accel Spectrom Detect Assoc Equip* 542(1–3):154–160
44. Zhao Q, Guo L, Wang Y, Jin H, Chen L, Huang Z (2020) Enhanced oil recovery and in situ upgrading of heavy oil by supercritical water injection. *Energy Fuels* 34(1):360–367
45. Shoji E, Kikuchi T, Yamagiwa K, Kubo M, Tsukada T, Takami S, Sugimoto K, Ito D, Saito Y (2020) In-situ visualization of heavy oil behavior in supercritical water using neutron radiography. *Chem Eng Sci* 225, Article number 115816
46. Balaskó M, Jancsó G, Kőrösi F (2004) Analyzing of segregation in mixtures of 3-methylpyridine and heavy water by dynamic neutron radiography. *Appl Radiat Isot* 61(4):597–602
47. Takenaka N, Asano H, Fujii T, Motomura Y, Ono A, Matsubayashi M, Tsuruno A (1996) Liquid metal flow measurement by neutron radiography. *Nuclear Instrum Methods Phys Res Sect A: Accel Spectrom Detect Assoc Equip* 377(1):156–160. ISSN 0168-9002
48. Mishima K, Hibiki T, Saito Y, Nakamura H, Matsubayashi M (1999) The review of the application of neutron radiography to thermal hydraulic research. *Nuclear Instrum Methods Phys Res Sect A: Accel Spectrom Detect Assoc Equip* 424(1):66–72

49. Saito Y, Mishima K, Tobita Y, Suzuki T, Matsubayashi M (2005) Measurements of liquid–metal two-phase flow by using neutron radiography and electrical conductivity probe. *Exp Thermal Fluid Sci* 29(3):323–330. ISSN 0894-1777
50. Khodarev E, Liquid metal fast breeder reactors. *IAEA Bull* 20(6)
51. Saito Y, Mishima K, Tobita Y, Suzuki T, Matsubayashi M, Lim IC, Cha JE (2005) Application of high frame-rate neutron radiography to liquid-metal two-phase flow research. *Nuclear Instrum Methods Phys Res Sect A: Accel Spectrom Detect Assoc Equip* 542(1–3):168–174. ISSN 0168-9002
52. Wolf F, Viskanta R (1987) *Experimental heat transfer*, vol 1, pp 17–30; Wang X, Fauelle Y (2009) *Int J Heat Mass Transfer* 52:5624–5633
53. Beckermann C, Viskanta R (1989) *J Heat Transfer* 111:416–424; Wolff F, Beckermann C, Viskanta R (1988) *Exp Thermal Fluid Sci* 1:83–91
54. Fife S et al (2003) *Exp Fluids* 35:152–158
55. Yin H, Koster JN (2003) *J Alloy Compd* 352:175–189
56. Barber PG et al (1986) *J Crystal Growth* 74:228–230
57. Chun J-H, Lanza RC, Saka N, Hytros MM (1995) *Ann CIRP* 44(1)
58. Mishima K, Fujine S, Yoneda K, Yonebayashi K, Kanda K, Nishihara H (1988) *Proc Japan-U.S. Seminar on Two Phase Flow Dynamics*, Ohtsu, Japan, pp C.3-1
59. Mishima K, Hibiki T, Nishihara H (1993) *Int J Multiphase Flow* 1:115
60. *Proc Seventh World Conference on Neutron Radiography*, Rome, Italy, 15–20 Sept 2002
61. *IEEE Trans Nuclear Sci* 52(1)
62. Kanematsu M, Maruyama I, Noguchi T, Iikura H, Tsuchiya N (2008) 3rd ACF international conference-ACF/VCA 2008, C 16, pp 925–931
63. Chalovicha TR, Bennett LGI, Lewis WJ, Brenizer JS Jr (2004) *Appl Radiat Isot* 61:693–700
64. Takenake N, Jujii T, Ono A, Motomura Y, Turuno A (1995) *Fusion Eng Des* 27:607–613
65. Ogino F, Kamata M (1994) In: Barton JP (ed) *Neutron radiography*, 4th edn. Kluwer, Dordrecht, pp 339–346
66. Reijonen H, Forsten J (1972) *J Cryst Growth* 12:61–62
67. Kumar L, Manjunath BS, Patel RJ, Prabhu SV (2014) Experimental investigations on melting of lead in a cuboid with constant heat flux boundary condition at two vertical walls using infra-red thermography. *Int J Heat Mass Transfer* 68:132–140
68. Sarkar P, Agrawal A, Kashyap Y, Shukla M, Sinha A, Kumar L, Manjunath BS, Prabhu SV, Markandeya SG (2013) Visualization of lead melting and solidification using neutron radiography. *Int J Nuclear Energy Sci Eng* 3(1)
69. Ito D, Saito Y, Sato H, Shinohara T (2017) Visualization of solidification process in lead-bismuth eutectic. *Phys Procedia* 88:58–63
70. Takenaka N, Kadowaki T, Kawabata Y, Sim CM, Nam KY (2002) Towards the visualization of fuel cavitation in a nozzle of a diesel engine by neutron radiography. In: *Proceedings of the seventh world conference*, Rome, Italy, 15–21 Sept 2002, pp 453–458
71. Takenaka N, Kadowaki T, Kawabata Y, Lim IC, Sim CM (2005) Visualization of cavitation phenomena in a Diesel engine fuel injection nozzle by neutron radiography. *Nucl Instrum Methods Phys Res, Sect A* 542(1–3):129–133
72. Vontobel P, Frei G, Brunner J, Gildemeister AE, Engelhardt M (2005) Dynamic imaging with a triggered and intensified CCD camera system in a high-intensity neutron beam. *Nucl Instrum Methods Phys Res, Sect A* 542(1–3):148–153
73. Brunner J (2021) Doctoral Thesis, Quantitative time resolved neutron imaging methods at the high flux neutron source FRM-II, <https://mediatum.ub.tum.de/doc/603123/603123.pdf>, accessed on 25/05/2021
74. Christian G (2013) Progress in industrial applications using modern neutron imaging techniques. 7th International topical meeting on neutron radiography. *Phys Procedia* 43:231–242
75. Gruenzweig C (2010) Visualization of a fired two-stroke chain saw engine running at idle speed by dynamic neutron radiography. *SAE Technical Paper* 2010-32-0013
76. Catchen GL, Hughes DE, Kulkarni AK, Ross KM, Ammerman WR (1987) Development of a neutron-radiographic technique for investigating physical models of fluidized beds. *Chem Eng Commun* 54(1–6)

77. Umekawa H, Ozawa M, Takenaka N, Matsubayashi M (1999) Visualization of bed material movement in a simulated fluidized bed heat exchanger by neutron radiography. *Nucl Instrum Methods Phys Res, Sect A* 424(1):77–83
78. Furui S, Umekawa H, Hayashi K, Ozawa M, Takenaka N (2002) Flow visualization of segregation process in a fluidized-bed by neutron radiography. Presented at the WCNR 7, Rome
79. Ozawa M, Umekawa H, Furui S, Hayashi K, Takenaka N (2002) Bubble behavior and void fraction fluctuation in vertical tube banks immersed in a gas–solid fluidized-bed model. *Exp Thermal Fluid Sci* 26(6–7):643–652
80. Umekawa H, Furui S, Oshima Y, Okura M, Ozawa M, Takenaka N (2005) Quantitative measurement of segregation phenomena in a binary-mixture fluidized bed by neutron radiography. *Nucl Instrum Methods Phys Res, Sect A* 542(1–3):219–225